Reaction-Induced Phase Separation in Crystallizable Micro- and Nanostructured High Melting Thermoplastic/Epoxy Resin Blends

Sara Goossens, Bart Goderis, and Gabriël Groeninckx*

Laboratory of Macromolecular Structural Chemistry, Department of Chemistry, Division of Molecular and Nanomaterials, Katholieke Universiteit Leuven, Celestijnenlaan 200F, 3001 Heverlee, Belgium

Received December 23, 2005; Revised Manuscript Received March 2, 2006

ABSTRACT: The phase-separation behavior of blends consisting of 4,4′-diaminodiphenylsulfone (DDS) cured diglycidyl ether of bisphenol A (DGEBA) with polyoxymethylene (POM) was investigated by means of small-angle laser light scattering (SALLS), optical microscopy (OM), and scanning electron microscopy (SEM). Curing results in reaction-induced phase separation (RIPS). Blends with different amounts of POM at curing temperatures above (180 °C) and below (150 and 145 °C) the melting temperature of POM (T_m = 168 °C) are considered. At an isothermal curing temperature of 180 °C, all blends demix according to a spinodal decomposition mechanism with the clear signature of viscoelastic effects at specific POM contents. Furthermore, curing leads to changes in the refractive indices of the phases, occasionally resulting in an apparent phase dissolution, which disappears again at the onset of secondary phase separation. Crystallization after curing at 180 °C can only be induced by cooling and is discussed using CTT diagrams for the blends with 10 and 20 wt % POM. Curing at 150 °C results in RIPS, preceding isothermal crystallization at the cure temperature. Curing at 145 °C induces isothermal crystallization in the homogeneous blend, followed by RIPS between the growing spherulites. At 145 °C a gradient of phase-separated structures is observed, when the growing spherulites sweep through the amorphous matrix where RIPS is in progress.

1. Introduction

Polyoxymethylene, POM, commonly known as polyacetal, is a linear, highly crystalline thermoplastic polymer. Because of the high crystallinity, POM exhibits excellent rigidity, hardness, and resistance to creep, fatigue, and chemical solvents. Because of its good mechanical properties and moderate cost, POM is among the most widely used engineering thermoplastics and hence can be considered as well-suited toughening agent for epoxy resins. Epoxy resins are, when fully cured, highly cross-linked, which make them inherently brittle and, as a consequence, limits their application possibilities. There are two major strategies for toughening epoxy resins: the first method consists of mechanically dispersing thermoplastic particles into the epoxy matrix. The second, and the most important strategy, is toughening the epoxy resins through phase separation upon curing.

Because of the increase of the molar mass of the epoxy resin during the cure reaction, phase separation occurs, as the entropic contribution to the Gibbs free energy becomes smaller, which finally results in a positive Gibbs free energy. This phenomenon is called reaction-induced phase separation (RIPS) and results in a thermoplastic-rich phase and an epoxy-rich phase. This multiphase morphology is able to initiate toughening mechanisms. As such, a thorough understanding of the formation of the phase morphology is of crucial importance for improving the mechanical properties of epoxy networks.

Curing of epoxy monomers leads to chain extension, branching, and network formation. As a consequence of this polymerization reaction gelation and vitrification may occur in the system. When the epoxy monomer is used in a blend system, next to the curing reaction RIPS can also occur due to the thermodynamic unstability of the system.[1−4] Experimental[2−11] and theoretical[12,13] studies were performed to investigate the phase-separation process, as this determines the final morphology of a thermoplastic/thermoset blend. If the system is quenched into the unstable or metastable part of the phase diagram, the phase-separation mechanism will depend on the position of the blend in the diagram and on the ratio of the rate of phase separation to the rate of the curing reaction. The importance of the curing cycle was demonstrated by Pascault et al., who generated conversion−temperature−transformation diagrams for poly(butylene therephthalate)−epoxy systems with different curing agents[5] and studied the different morphologies, developed by different cure cycles.[6]

Thermoplastic/thermosetting polymer blends, exhibiting both phase separation and crystallization, are of particular interest since their morphology and properties can be influenced by both processes. By choosing a thermoplastic component with melting and crystallization temperatures in the temperature range of the curing epoxy oligomers, phase separation can be influenced by the isothermal crystallization of the thermoplastic polymer and vice versa. Up to now, research on epoxy systems containing a crystallizable component was primarily focused on the crystallization behavior and morphology of the thermoplastic in the cured or uncured system.[14−22] In our group the crystallization behavior of the low melting poly(ϵ-caprolactone)/DGEBA/4,4′-diaminodiphenylsulfone blends was studied by DSC and discussed with respect to the RIPS and the resulting morphologies.[20] Schut et al.[21,22] studied an epoxy system modified with a high melting polymer, namely syndiotactic polystyrene (sPS) (T_m = 270°C), which has a much higher melting point and hence is more difficult to process than the thermoplastic we use. In this study, the choice of the thermoplastic POM makes it possible to investigate the interrelation between the liquid−liquid demixing process and the crystallization, using different isothermal curing temperatures to influence both RIPS and crystallization. Changing the curing temperature will affect the occurrence of isothermal crystallization and the rate and mechanism of RIPS.

* Corresponding author. E-mail: gabriel.groeninckx@chem.kuleuven.be. Telephone: +32-16-327440. Fax: +32-16-327990.

10.1021/ma052742o CCC: $33.50
Published on Web 03/24/2006

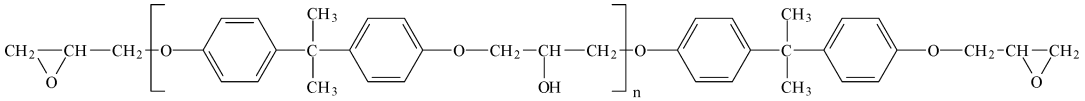

DGEBA

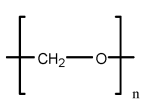

POM

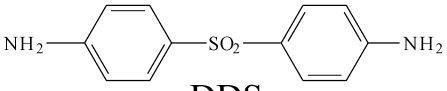

DDS

Figure 1. Chemical structure of DGEBA, DDS, and POM.

Often the same dynamics for the two components in a demixing thermosetting blend are assumed in conventional studies, although the size of the molecules involved at the beginning of the phase-separation process is clearly different, i.e., small epoxy oligomers and large POM polymers. This is called "dynamic asymmetry". This asymmetry induces unusual phase morphologies, like the spongelike phase inversion structure and the moving droplet phase.[23−26] This so-called viscoelastic phase separation was first reported by Tanaka et al..[27] For dynamic asymmetric systems a so-called "dynamic phase diagram" was proposed, where a dynamic symmetry line determines the threshold between the normal and viscoelastic phase separation. For shallow quenches, the normal phase separation can be observed and the conventional phase diagram can be used. For deep quenches, viscoelastic phase separation occurs. Between both mechanisms, a transition zone is present. In the present context, detecting viscoelastic phase separation would point at a fast shift of the phase diagram, induced by the polymerization reaction of the growing thermoset. In fact, viscoelastic phase separation seems to be a universal phenomenon, present in all dynamically asymmetric mixtures.[28] The interplay between the phase-separation dynamics and the slow dynamics of the material itself determines extensively the phase-separation process. The slow polymer component cannot catch up with the deformation rate of the phase separation and starts to behave like a viscoelastic body.

2. Experimental Section

2.1. Materials. The epoxy resin used was a low molar mass liquid diglycidyl ether of Bisphenol A (DGEBA) (Epikote 828VEL, EEM 182−187 g, ICI, Belgium) with an epoxide equivalent weight of 5,36 mol/kg. The hardener used was 4,4′-diaminodiphenylsulfone (DDS) (Sigma-Aldrich, A7, 480−7, M_w = 248 g/mol), and the crystallizable thermoplastic component was polyoxymethylene (POM) (Hostaform C9021 naturel, T_m = 168 °C, T_c = 138 °C), modified with a sterical hindered phenol, used as an antioxidant. The end groups are stabilized with the comonomer dioxolane to increase the thermal stability. POM was kindly provided by Ticona, Benelux. The chemical structures of DGEBA, DDS, and POM are given in Figure 1.

2.2. Sample Preparation. The blend preparation occurred in three steps. First, the thermoplastic component was added to the epoxy monomer at 180 °C under stirring, until a homogeneous mixture was obtained. Next, DDS was added to this mixture in the stoichiometric ratio of epoxy to amino hydrogens equal to 1 under continuous stirring for approximately 30 s. Finally, the mixture was quenched for 1 min in liquid nitrogen to minimize the epoxy conversion before the actual measurements started. Blends of 5, 10, 15, 20, and 30 wt % POM were prepared with this melt-mixing method. Compositions above 30 wt % POM could not be made, because the reaction mixture became too viscous to stir properly.

2.3. Techniques. 2.3.1. Optical Microscopy. Optical microscopy (OM) was used to investigate the behavior of the DGEBA/POM/DDS blends visually. Measurements were performed on an Olympus BH_2 microscope equipped with cross-polarizers. Samples of several mg were put between two glass slides and placed in a Mettler FP82-HT hot stage. Digital micrographs were taken at several curing times by a JVC TK-C1381 CCD camera and analyzed by the program Qwin from Leica Company. The phase separation and isothermal crystallization of POM were studied at 180, 150, or 145 °C.

2.3.2. Small Angle Laser Light Scattering. The small angle laser light scattering (SALLS) setup used comprises a linear polarized 1 mW Spectra-Physics 117A type He−Ne laser (λ = 632,8 nm), a polarizer set parallel to the laser polarization, the sample in a Mettler FP-82HT hot stage, a second polarizer (analyzer), a screen with a beam catcher on which the scattering patterns are projected, and a Photometrix ATC200L cooled CCD camera as detector. The scattering angles were calibrated using a 100 lines/mm grid and expressed as q ($q = (4\pi/\lambda)\sin(\theta/2)$), where q is the modulus of the scattering vector, λ the wavelength of the laser light and θ the scattering angle. Samples of a few milligrams were put between two microscope glass slides and placed into the Mettler oven to examine the phase-separation process and/or the crystallization. During the measurements the analyzer was alternated between parallel (Vv-setup) or perpendicular (Hv-setup) to the polarizer using a flipper. The scattered intensity was recorded as a function of time on a PC. Every 15 s a picture was taken, which alternately is an Hv or Vv image. Processing of the data was performed with a homemade script running under V for Windows (version 3.5b, Digital Optics Ltd.). The software takes care of the integration of the scattered intensities, which results in the relative total light scattering intensity (Q_{Hv} and Q_{Vv} for the Hv and Vv setup respectively) and an azimuthal averaging of the 2D Vv patterns. Analysing the scattering patterns led to the determination of the onset and mechanism of the phase separation and the onset of crystallization.

2.3.3. Scanning Electron Microscopy. To examine the phase morphology of the different blends, scanning electron microscopy was used. SEM pictures were taken with a Philips XL20 Series SEM. At first, the samples were fractured in liquid nitrogen, avoiding deformation at break. Next, they were etched with benzyl alcohol at 136 °C to remove the thermoplastic component POM and finally dried overnight under vacuum to remove any residual solvent. Each sample was coated with a thin gold layer to improve the electron conductivity during the SEM measurements.

2.3.4. Differential Scanning Calorimetry. Dynamical DSC measurements were performed using a DSC 7 from Perkin-Elmer, purged with dry nitrogen gas. Enthalpy calibration was performed with indium. Temperature calibration was done with benzophenon and indium. The sample mass varied between 2 and 5 mg. A different approach was utilized for curing above and below the melting temperature of POM. For an isothermal curing temperature (T_{cure} = 180 °C) above T_m of POM the following procedure was used: first, the samples were cured for a certain time at 180 °C; subsequently, they were cooled to −10 °C at a rate of 40 °C/min and heated again at the same speed to minimize extra curing during the dynamical experiments. The heating step was used to determine the T_g (the midpoint of the heat capacity change was taken as T_g) and the maximum of the endothermic peak was taken as the melting temperature (T_m). The minimum of the exothermic peak during

Table 1. Overview of the Onset Times and Mechanisms of the Phase Separation during Curing at 180 °C and Final Morphologies after 4 h of Curing at 180 °C

wt % POM	onset time RIPS (min) (±0.5 min)	mechanism	morphology
5	10.2	spinodal	particle-matrix; epoxy = matrix
10	10.5	spinodal	particle-matrix; epoxy = matrix
15	10.4	spinodal	co-continuous
20	12.1	spinodal	phase-inverted; POM = matrix
30	12.6	spinodal	phase-inverted; POM = matrix

cooling was assigned as the crystallization temperature (T_c). Displaying these parameters as a function of the conversion degree one obtains "conversion−temperature−transformation" (CTT) diagrams. To establish the thermal transitions, a fresh sample was used for each conversion degree. The same measuring conditions were applied for the conversion determination, but the measurements were performed on a Perkin-Elmer Pyris 1 DSC. The conversion degree, α, at a given time t was determined by dividing the heat ΔH_t during isothermal cure up to that particular time t by the total exothermic heat of the epoxy−amine reaction ΔH_{total} equal to 408 J/g.

For the samples cured below the T_m of POM (at 150 and 145 °C), an additional step was added: prior to the isothermal curing, the samples were heated for 1 min at 180 °C to melt the POM in the blends. Next, the samples were cooled to the isothermal curing temperature (150 or 145 °C) at a rate of 40 °C/min. Finally, after a predetermined time at the isothermal cure temperature the blends were cooled and heated again, similar to those cured at 180 °C in order to obtain T_g, T_c and T_m. However, only the results obtained for curing at 180 °C will be discussed in this paper for reasons mentioned in the result section.

3. Results

3.1. Curing above the Melting Point of POM (at 180 °C). 3.1.1. Reaction-Induced Phase Separation. RIPS in the DGEBA/POM/DDS blends, cured isothermally at 180 °C, was investigated with optical microscopy and SALLS. The onset times and the mechanism of RIPS for the different blends are presented in Table 1. Onset times were determined as the data point at the first increase of the Vv-scattering intensity and are more or less constant for the blends with from 5 up to 15 wt % POM. Increasing the amount of POM further, increases the onset time of RIPS. Blends with from 5 up to 30 wt % POM demix according to the spinodal mechanism.[2,4,10] For all these blends, a cocontinuous structure was observed at the beginning of phase separation. The final blend morphologies of the different blend compositions after 4 h curing differ because of their position with respect to the critical point[1] and are summarized in Table 1. Figure 2 shows the three different morphologies after 4 h of curing at 180 °C: blends with 5 and 10 wt % POM exhibit a particle/matrix structure with POM-rich particles dispersed in the epoxy-rich matrix (Figure 2a). 15 wt % POM exhibits a cocontinuous morphology (Figure 2b,c). Both continuous phases underwent secondary phase separation: the continuous epoxy-rich phase exhibits dispersed POM-rich droplets and the continuous POM-rich phase displays small dispersed epoxy-rich droplets. Figure 2b is an OM picture of the blend with 15 wt % POM, showing the phase morphology at a small magnification to get a general view of the structure. The SEM picture in Figure 2c is a view of the same blend at a larger magnification (the scale bar in Figure 2a holds for all SEM pictures in Figure 2). Blends with from 20 up to 30 wt % POM have a phase-inverted structure with the POM-rich phase as matrix (Figure 2d). Before taking the SEM pictures, the POM-rich phase was dissolved, and as a result, the structures in the pictures represent only the epoxy-rich phase. The phase-separation process was studied in detail by OM.

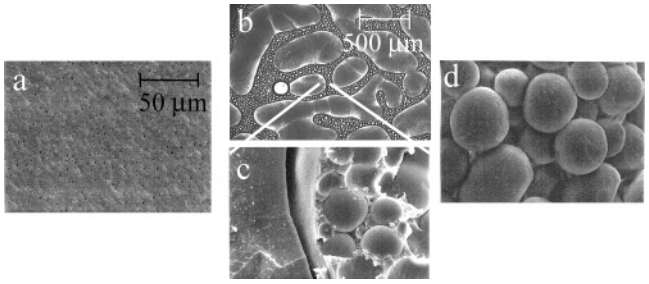

Figure 2. Blend morphologies after 4 h of curing at 180 °C: (a) 5 wt % POM (SEM), (b) 15 wt % POM (OM), (c) 15 wt % POM (SEM), and (d) 30 wt % POM (SEM).

The optical microscopy pictures in Figure 3 illustrate the main morphological changes happening in a 10 wt % POM blend during phase separation. After 10 min, a cocontinuous structure is formed (Figure 3a). After 2 or 3 min, this cocontinuous structure breaks up in POM-rich droplets, dispersed in an epoxy-rich matrix (Figure 3b). With time this morphology coarsens due to ripening: larger droplets develop at the expense of smaller ones and the total number of droplets decreases (Figure 3c). For a blend with 5 wt % POM, the demixing behavior is similar to that of the 10 wt % POM blend. The initial cocontinuous structure converts into a droplet/matrix structure.

The phase-separation process for the 15 wt % POM blend is depicted in Figure 4. The morphological changes are typical of viscoelastic phase separation and can be described as follows. At the start of the spinodal phase separation, the amplitude of concentration fluctuations grows and a cocontinuous structure is observed (Figure 4a). However, at a given time viscoelastic effects prevent the growth of the composition fluctuations and the system temporarily freezes. In the next step, the epoxy-rich phase, which at this moment is the least viscous part, starts to form holes, which grow with time (Figure 4b,c), indicating the transport of the epoxy oligomers from the small-scale separated (POM-rich) matrix toward the epoxy-rich holes. The slower dynamic POM-rich matrix finally behaves as an elastic body with the progressive escape of the epoxy oligomers. In the elastic regime, the elastic force balance dominates the morphology instead of the interfacial tension, which leads to the corrugated shape of the domains (Figure 4d,e). In the final stage, the driving force associated with the interfacial energy overcomes the elastic energy and the domains become more rounded (Figure 4f). At first sight, the small-scale separated nature of the matrix is preserved at all time. With time, this separated local morphology evolves to a clearly continuous POM phase with dispersed epoxy-rich droplets as illustrated in Figure 4f. In the end, SEM pictures also reveal the presence of small POM droplets in the large epoxy-rich holes, pointing at secondary phase separation. For this blend the POM concentration is not high enough to keep the inversed structure, induced by the primary phase separation. Because of the growth of the epoxy-rich domains a continuous epoxy-rich phase is finally formed and the overall morphology is cocontinuous.

The Vv intensity as a function of time (Figure 5a) and as a function of q (Figure 5b) shows the different morphological changes during the phase-separation process. At first, a peak at large angles—typical of spinodal phase separation—appears and shifts quite rapidly toward smaller angles (Figure 5b). This is reflected in the steep increase of the Vv-scattering intensity at the beginning of RIPS (Figure 5a). Once the epoxy holes start to form and grow, an intensity decrease is observed in the

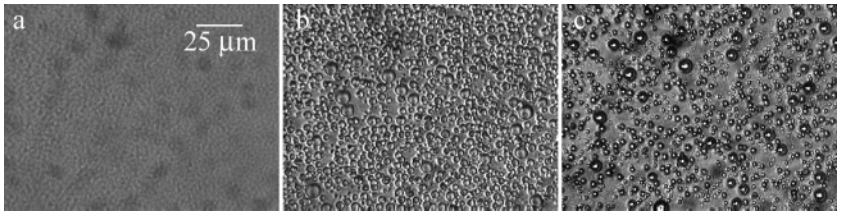

Figure 3. OM pictures of the phase separation of a blend with 10 wt % POM at 180 °C: (a) after 11, (b) 14, and (c) 60 min of curing.

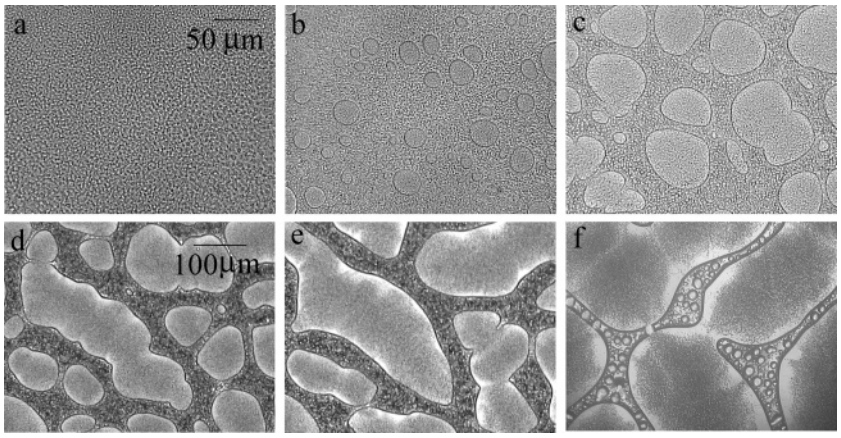

Figure 4. OM pictures of a blend with 15 wt % POM cured during different times at 180 °C: (a) 10.75, (b) 11.25, (c) 11.75, (d) 12.5, (e) 13.5, and (f) 60 min.

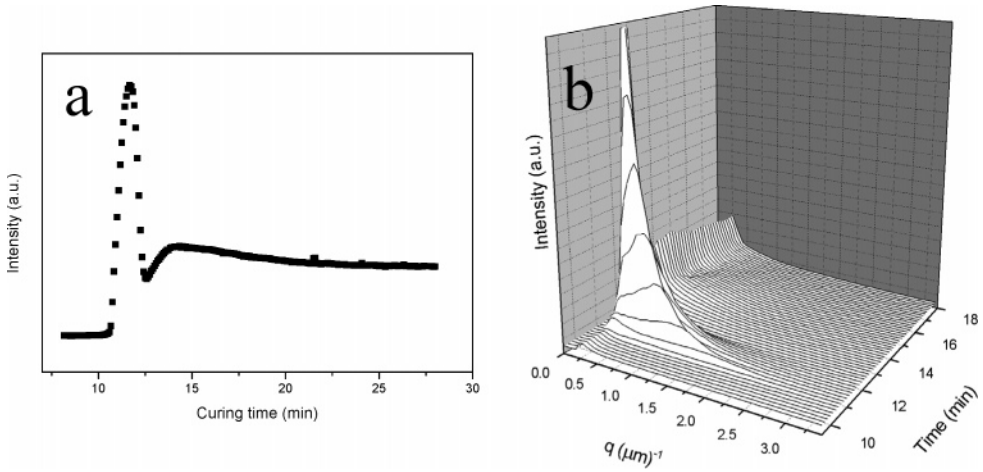

Figure 5. (a) Intensity vs curing time plot of a 15 wt % POM blend cured at 180 °C with (b) the corresponding scattering profile.

scattering profiles. The epoxy-rich holes are readily too large to contribute to the scattering in the experimental *q*-window. Accordingly, this decrease points to a lowering of the refractive index contrast between the constituting phases of the (small-scale separated) matrix or to a progressive homogenization (remixing) within this matrix. After 12.5 min, the intensity rises again, and this event coincides with the appearance of less corrugated phases (Figure 4e). In the meantime, the small epoxy-rich droplets within the matrix phase become more apparent. Considering all events it is conceivable that—as soon as the larger epoxy holes form—the small-scale phase-separated matrix phase starts to homogenize because of the progressive extraction of epoxy oligomers. Subsequently, because of the ongoing reaction, a secondary phase separation occurs within the homogenized matrix phase by which the POM-rich continuous phase in contact with the large epoxy-rich holes is suddenly enriched with POM. Concomitantly, the interfacial tension between the matrix phase and the epoxy-rich holes increases, leading to more rounded surfaces. In the scattering profile, a shoulder at small angles appears, compatible with the genesis and growth of these secondary epoxy-rich particles. As all events follow very closely, it appears from optical microscopy as if the small-scale phase-separated nature of the matrix phase is preserved all the time.

OM pictures of the phase-separation process of a blend with 20 wt % POM are shown in Figure 6. Similar to the previous blends, a cocontinuous structure is formed at the beginning of the RIPS (i.e., after 12.1 min of curing), indicating spinodal demixing. One minute after the onset of phase separation, the epoxy-rich phase forms holes, which coalesce and grow (Figure 6a). One minute later, the epoxy-rich droplets seem to fade away in the POM-rich matrix (Figure 6b) and after two more minutes large epoxy holes suddenly appear again that *very rapidly* grow with time (Figure 6c). This sequence of events suggests that the refractive indices of both phases are crossing each other, seen as an "apparent phase dissolution" and a subsequent reappearance. Inoue studied a thermoset/thermoplastic blend of which the refractive index of the pure components was measured by means of ellipsometry.[4] At the end of the curing reaction, the refractive index of the thermoset was identical or very close

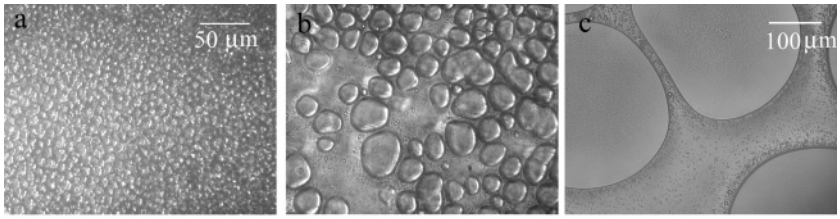

Figure 6. OM pictures of the development of the phase morphology for a blend with 20 wt % POM after (b) 12, (c) 14, and (d) 60 min of curing at 180 °C.

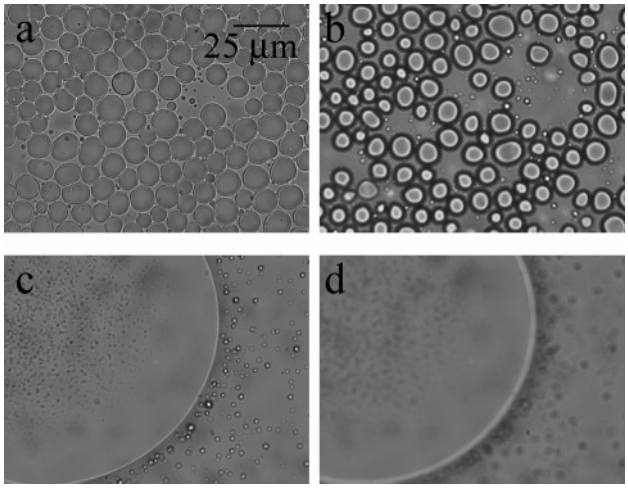

Figure 7. Becke Line test for the blend with 20 wt % POM cured at 180 °C. First kind of epoxy holes (a, b): (a) in focus; (b) with distance between specimen and objective increased. Second kind of epoxy holes (c, d): (c) in focus; (d) with distance between specimen and objective increased.

to that of the thermoplast, i.e., poly(ether sulfone). Because of this similarity in refractive index, the total light-scattering intensity (associated with the presence of different phases) vanishes at the end of the curing reaction and the term "apparent phase dissolution" was coined.[4] When the refractive indices of the components are very close but do no not exactly match, the light-scattering intensity rises again after the extinction due to crossing phase refractive indices.

However, the refractive indices of the phases do not cross in the present case and accordingly another explanation for the "apparent phase dissolution" and subsequent reappearance needs to be looked for. Using "the Becke Line approach",[29] it could be concluded that the refractive index of the dispersed (epoxy-rich) phase is the largest before as well as after the apparent phase dissolution (the phase assignment is based on cooling experiments in which only the continuous POM-rich phase crystallizes) as the (bright) Becke Line is invariably moving inside the droplets when the distance between the specimen and objective is increased (Figure 7). We can explain this by considering the composition change of the POM-rich phase and the fact that the refractive index of POM[30] is the lowest followed by that of the epoxy monomers and finally that of the cured epoxy. The refractive index of a given phase is determined by the fractional composition of the three components. Therefore, the match of the refractive indices (at the apparent phase dissolution) suggests very similar phase compositions and, accordingly, the proximity of a critical point. At the beginning of the phase separation, small epoxy molecules—in fact, essentially monomers—are present in the POM-rich phase[31,32] and polymerize upon curing. This will increase the refractive index of the POM-rich phase, approaching that of the epoxy-rich phase, and the epoxy holes disappear.

However, upon further curing, the growing molecules in the POM-rich phase will at a given moment be excluded, due to a secondary phase separation. Small epoxy-rich particles are generated and the refractive index of the POM-rich matrix phase decreases again, resulting in the reappearance of large epoxy-rich droplets. Note that there is seemingly little or no tendency for coalescence at the stage prior to the reappearance of the epoxy holes, pointing at a very low surface tension between the two phases and thus similar phase compositions. When the epoxy-rich holes reappear, coalescence is, however, *very rapid (and hard to record)*. This indicates not only that secondary phase separation reestablishes the refractive index differences between the phases but also that due to the enhanced compositional difference between the epoxy-rich holes and the POM-rich matrix, the surface tension has increased. At the critical point, the phase volume occupancy should be close to 50%. This is not obvious from the numerous droplets in Figure 6a, but one should keep in mind that the sample thickness by far exceeds the diameter of the droplets and that accordingly a projection is seen of droplets at different heights within the sample volume. The phase volume fractions after coalescence indeed approach the expected 50% level (Figure 6c). It therefore seems that the small-scale secondary phase separation did not significantly alter the volume fractions of the primary phase-separation process. When we compare the final phase morphology of the 20 wt % POM blend with the one of 15 wt % POM (Figure 4f), very clearly in the latter case the phase volume fractions are further away from 50% occupancy. Furthermore, in the latter case, the phase compositions are too dissimilar to induce the effect of apparent phase dissolution.

Figure 8 shows the OM pictures of the initial phase-separation process of a blend with 30 wt % POM. After the cocontinuous structure (Figure 8a) has developed, epoxy-rich holes emerge that after some growth (Figure 8b) disappear (Figure 8c), comparable to the blend with 20 wt % POM. Also in the SALLS-intensity plots of the blends, not shown here, a sudden decrease of the scattering intensity can be observed. Similar to the blend of 20 wt % POM the epoxy-rich droplets reappear after some time (not shown here). The Becke Line approach indicates again that the refractive indices of the phases are first approaching, then reaching a minimum, and finally increasing again. After 4 h of curing, these blends result in a phase-inverted structure with interconnected epoxy droplets dispersed in a POM-rich matrix. The epoxy droplets formed in the 30 wt % POM blend are smaller compared to those of the 20 wt % POM blend. The observation of an apparent phase dissolution points at very similar phase compositions and accordingly the proximity of a critical point.

3.1.2. Conversion—Temperature—Transformation (CTT) Diagram. When the blends are cooled from 180°C and heated again, crystallization, respectively melting of POM occurs at the crystallization (T_c) and melting temperature (T_m). The extent of curing of the epoxy monomer (reflected in a continuously increasing glass transition temperature (T_g)) and the instanta-

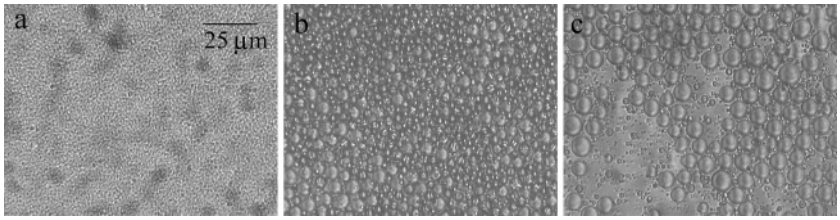

Figure 8. OM pictures of RIPS for a blend with 30 wt % POM after (a) 14, (b) 21, and (c) 25 min of curing at 180 °C.

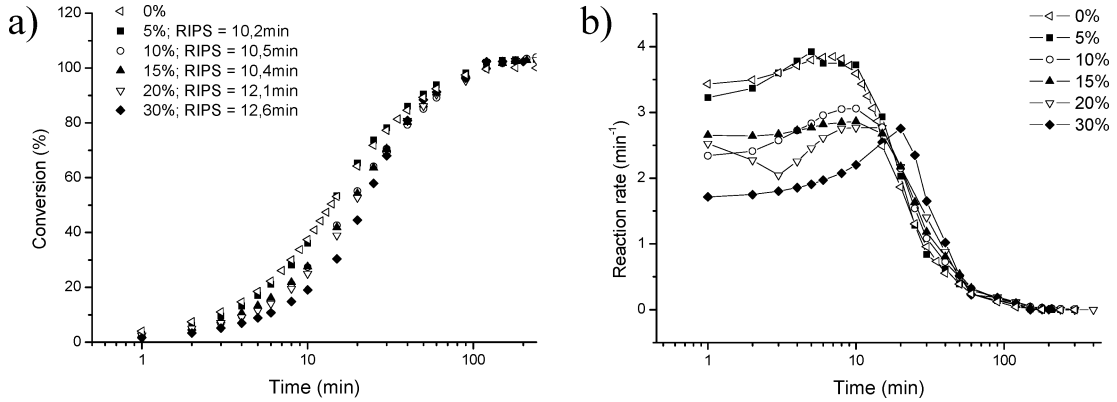

Figure 9. (a) Conversion degree of different blend systems and neat epoxy cured at 180 °C (the time at phase separation is added to the legend) and (b) the corresponding reaction rates.

neous phase morphology influence the crystallization of POM. Furthermore, according to the literature, there is a continuous enrichment of both phases in the main component after the onset of phase separation,[1,31−33] implying that, when cooling at a given moment during the cure process, the crystallization and melting temperature of the POM-crystallites formed, should increase when the curing time is increasing. During cooling *prior* to exhausted curing, the cooling process will slow down the ongoing reaction as well as the phase morphology development, in particular when the instantaneous T_g is reached during cooling. Obviously, the phase morphology development is also affected *when crystallization occurs* prior to vitrification. These mutual influences are best expressed in a conversion−temperature−transformation (CTT) diagram.

Figure 9a displays the conversion of the different blends in function of time when cured at 180 °C. The time at phase separation is indicated in the legend to this figure as RIPS. Before phase separation sets in, blends with a higher amount of POM exhibit a lower conversion degree than those with a lower amount, because the reacting chemicals are progressively diluted and because the mixture becomes increasingly more viscous with increasing amount of POM-polymers. Once phase separation occurred, the difference in conversion degree becomes smaller, and finally no significant differences in conversion degree are detected at the end of the cure reaction. In Figure 9b, the corresponding reaction rates of the different systems are calculated as $d\alpha/dt$. Before phase separation sets in, increasing the amount of POM decreases the reaction rate epoxy/amine in the homogeneous system, because of the dilution of the reactive species. For all compositions, the reaction rate increases with time prior to phase separation, reflecting the autocatalysis associated with the formation of the hydroxyl groups.[34,35] Adding more POM, increases the time needed to reach the maximum reaction rate. The maximum of the reaction rate is situated before RIPS for the blend with 5 wt % POM; for the 10, 15, and 20 wt % POM blends, the maximum coincides with the onset of phase separation. For the 30 wt % POM blend, the maximum of the reaction rate is situated after RIPS sets in. This increase in reaction rate after RIPS for blends with relatively high concentrations of thermoplastic modifier has been observed previously by Bonnet et al.[36] and was explained by the increase in concentration of reactive groups in the epoxy-rich phase. Increasing the amount of POM has a diluting effect, which is relatively reduced after phase separation. For the lower concentrations of POM, this difference in concentration of reactive groups after phase separation is so small that the reaction acceleration is dominated by the autocatalysis. The conversion degrees of the different blends at the onset of RIPS are 36% for the 5 wt %, 27% for the 10 wt %, 28% for the 15 wt %, 26% for the 20 wt %, and 23% for the 30 wt % POM. These results can be discussed in terms of the reaction rates. The 5 wt % POM blend displays the largest conversion degree at the RIPS. Figure 9b illustrates that for this blend the maximum of the curing rate is situated before the RIPS. The conversion degree at the RIPS of the blends with from 10 up to 20 wt % POM are virtually identical and for all of them the maximum of the reaction rate occurs around the onset of RIPS. The 30 wt % POM blend conversion degree at RIPS is lower than for the others, and it is observed that the reaction rate maximum for this blend occurs after the onset of RIPS. Finally a decrease in reaction rate can be observed for all blend compositions due to a progressive reduction of reactive groups until full conversion is reached.

Figure 10 shows two conversion-temperature-transformation (CTT) diagrams for blends with 10 and 20 wt % POM cured at 180 °C (Figure 10, parts a and b, respectively). The T_g values are extracted from the DSC heating runs and are associated with the epoxy-rich phase and accordingly are only reported after phase separation. It is clear that the liquid−liquid phase separation occurs well before vitrification of the epoxy-rich phase sets in, i.e., at overall conversions above 80% (see open diamonds in Figure 10a). The local conversion in the epoxy-rich phase is likely even larger. The crystallization temperatures after the onset of phase separation are associated with the crystallization of POM in the POM-rich phase (T_c, and T_c* for the 10 wt % blend and T_{c1} and T_{c2} for the 20 wt % blend).

At first sight optical microscopy does not reveal any crystallization in the epoxy-rich phase for the 20 wt % POM

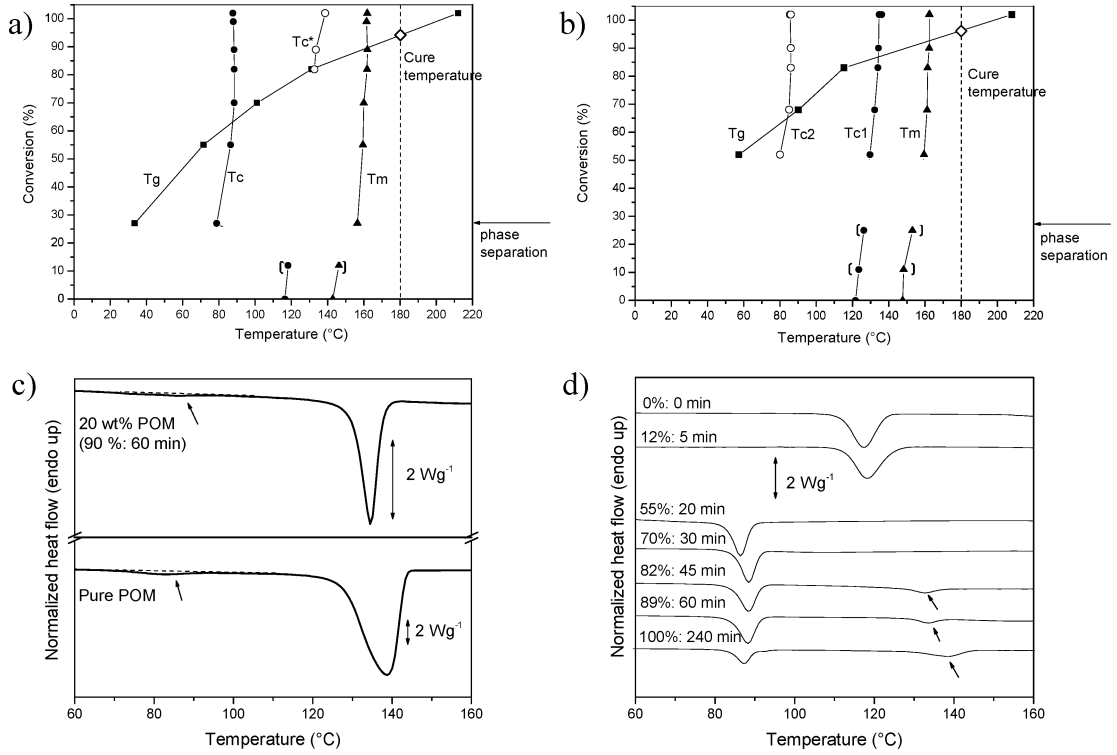

Figure 10. CTT diagrams of blends containing 10 (a) and 20 wt % POM (b). (c) Comparison between the cooling curves of a blend of 20 wt % POM cured for 60 min at 180 °C and pure POM (the arrows highlight the homogeneous nucleation). (d) Cooling curves of a blend of 10 wt % POM cured for different times at 180 °C. The arrows point to the small exothermic peaks at smaller supercooling than the main crystallization peaks at around 85 °C.

sample. However, a very small exothermic peak is observed close to 80 °C (T_{c2}, represented by open circles in Figure 10b). This crystallization event is most likely associated with the (homogeneous) crystallization of POM in the POM-rich droplets realized by secondary phase separation within the primary epoxy-rich phase. The size of these droplets is very small, explaining why their crystallization escapes the observation in optical microscopy. Figure 10c illustrates that a small crystallization peak at about 80 °C also appears in *pure POM* during cooling at 20 °C/min. Quite often such a small peak is present 30 °C below the main crystallization peak in the case of *pure* linear poly(ethylene) and ethylene copolymers with a moderate comonomer content and has tentatively been attributed to the *homogeneous* nucleation and crystallization of molecules that got trapped and separated from the primary crystals.[37] The present data support this view, assuming that POM and poly(ethylene) behave similarly. Homogeneous nucleation is supported here in particular because the crystallization temperature (T_{c2}) of the separated POM droplets that have to nucleate independently (homogeneously), coincides with the temperature at the small secondary exothermic peak in pure POM.

Additional support for the latter view can be found in the data related to the 10 wt % sample. T_{c2} of the 20 wt % sample occurs at the same temperature where POM crystallizes in the 10 wt % sample after demixing (T_c in Figure 10a). Indeed, for this blend, a sudden decrease of the crystallization temperature at the moment of phase separation can be observed, due to the phase morphology: POM-rich particles are dispersed in an epoxy-rich matrix, and crystallization needs to be induced by the independent, homogeneous nucleation within each POM-rich droplet.[38] Homogeneous nucleation requires a large supercooling compared to heterogeneous nucleation. For the 20 wt % blend, a single, heterogeneous (high-temperature) nucleation event can induce crystallization over a large sample volume in the POM-rich matrix phase.

In Figure 10a, it can be seen that at around 62% of conversion the T_g of the epoxy-rich phase becomes higher than the T_c of the POM-rich phase. Concomitantly, a new crystallization peak starts to develop at T_c*. Figure 10d illustrates that the area covering the latter crystallization peak, becomes progressively larger at the expense of crystallization that is occurring at T_c after 62% conversion. On this account, it is tempting to assign this high-temperature crystallization to some nucleating activity of the vitrified matrix. However, if so, one expects a much more massive effect, as nucleation would be induced in *all* droplets and crystallization at T_c would disappear completely. Therefore, this connection with the matrix T_g seems accidental. The true origin of T_c* can be found in the optical microscopy data of Figure 3. Clearly, the initial droplet morphology coarsens with time by ripening. The larger droplets that contain heterogeneous nuclei can trigger crystallization in a larger volume, by which the extent of a "bulk-like" crystallization grows as coarsening proceeds. Isothermal coarsening at 180 °C can progress up to a vitrification of the matrix phase at this particular temperature, which is at 95% conversion or after approximately 100 min.

The POM enrichment in the "POM-rich" phase due to phase separation is moderate in the 20 wt % sample since the crystallization temperature (T_{c1}) is not much different from that of the mixed blend at zero conversion. This implies a comparable POM concentration in both phases, which was also deduced from the observation of apparent phase dissolution. The expected increase of the crystallization (cooling) and the melting temperature (heating again) with increasing curing time after the RIPS is also small and accordingly, an enrichment of the POM-rich phase with POM polymers during curing is not very pronounced (this also holds for the 10 wt % sample as seen from the evolution of T_c). Moreover, this is compatible with the preservation of phase volume fractions during the phase morphology development as explained for the 20 wt % POM sample. Note that T_{c1} and T_m also slightly increase *prior* to the

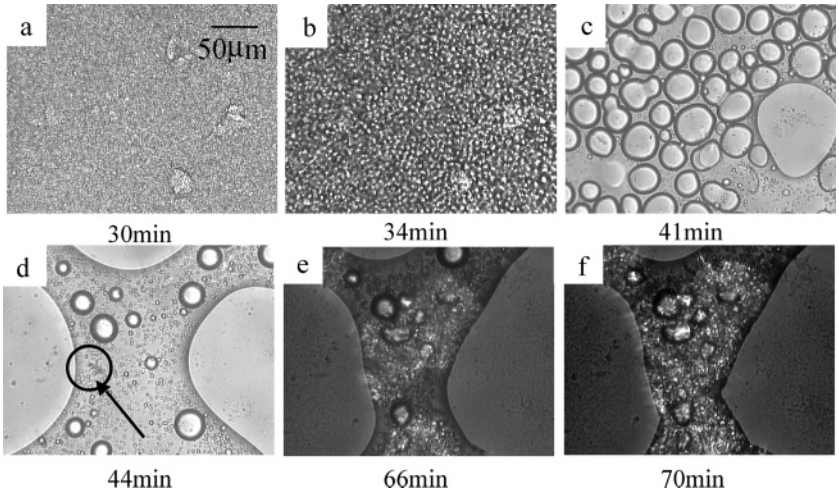

Figure 11. OM pictures of a blend with 20 wt % POM, cured for 2 h at 150 °C. RIPS is followed by isothermal crystallization inside the POM-rich phase. The arrow indicates the start of a growing spherulite.

Table 2. Overview of the Onset Times of RIPS and Isothermal Crystallization, Mechanisms of Phase Separation during Curing at 150 °C and Morphologies after 4 h of Curing at 150 °C

wt % POM	onset time of RIPS (min) (±0.5 min)	onset time of isothermal crystallization (min) (±0.5 min)	mechanism of RIPS	morphology
5	28.9		spinodal	particle-matrix; epoxy = matrix
10	30.2		spinodal	particle-matrix; epoxy = matrix
15	29.2	41.4	spinodal	phase-inverted; POM = matrix
20	31.4	45.0	spinodal	phase-inverted; POM = matrix
30	34.8	55.1	spinodal	phase-inverted; POM = matrix

onset of phase separation *at 180* °C. It will be argued below that demixing in the present case has UCST characteristics (upper critical solute temperature) and that the upper critical solution temperature is shifting to higher temperatures with increasing conversion. Therefore, it is conceivable that demixing is induced at very small conversion during the DSC cooling run and that this happens—depending on the extent of curing—after, during, or before the crystallization onset. A full discussion of this particular aspect of "mutual influence" between demixing and crystallization, established *during a cooling run* goes beyond the scope of this paper and will be discussed elsewhere. To emphasize the present lack of information under these conditions, the corresponding T_{c1} and T_m data points are put in brackets in Figure 10b. The same holds for some data points related to the 10 wt % blend (Figure 10a).

Relevant to this paper, however, is the competition between isothermal crystallization and LLPS for the cure temperatures of 150 and 145 °C. Putting up CTT diagrams in the latter cases was not possible since the exothermic signal in the isothermal DSC-measurements is a too strong overlap of both the heat released by crystallization and curing.

3.2. Curing below the Melting Point of POM. Lowering the curing temperature from 180 to 150 or 145 °C makes isothermal crystallization of POM possible, because T_{cure} is then situated below the melting point of the thermoplastic component. As a result, isothermal crystallization will interfere with RIPS. The crucial question at this point is if the liquid−liquid-phase separation will precede the isothermal crystallization or vice versa and what the impact will be on the morphology development. In the next section the first results of the study on this mutual influence are presented and discussed.

3.2.1. Curing at 150 °C. After POM in the blends was melted for 1 min at 180 °C, the blends were cooled to 150 °C at 40 °C/min and cured at this particular temperature. Figure 11 shows

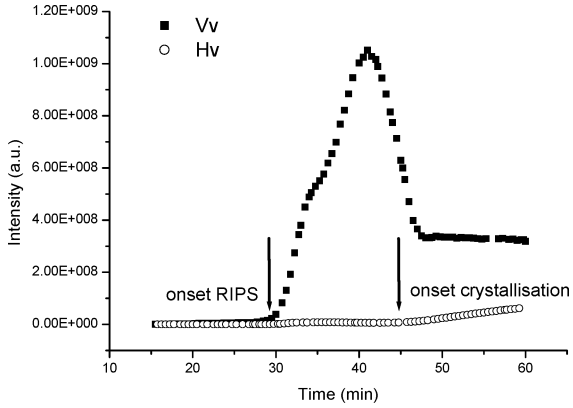

Figure 12. Intensity vs time plot of a blend with 20 wt % POM, cured for 1 h at 150 °C, obtained with SALLS: Vv and Hv signals.

optical microscopy pictures of a blend with 20 wt % POM, which indicates that RIPS starts before the isothermal crystallization does. Parts a−c of Figure 11 display the phase-separation process, beginning with the formation of a cocontinuous structure, followed by the creation of epoxy droplets and the subsequent formation of solvent holes, which grow in size, similar to the blend with 20 wt % POM at 180 °C. After 44 min, inside the POM-rich phase, isothermal crystallization starts (shown in Figure 11d and indicated with an arrow). Parts e and f of Figure 11 illustrate the progressing crystallization in the POM-rich phase, which has been photographed with partially crossed polarizers to improve visibility of the growing crystal aggregates. Some epoxy droplets seem to display a little birefringence, but actually this is not the case since measurements showed that this is due to the growth of matrix spherulites over the droplets. Both processes can also be observed with SALLS measurements. Figure 12 displays the intensity vs time plot for a 20 wt % POM blend, cured for 1 h at 150 °C. In the

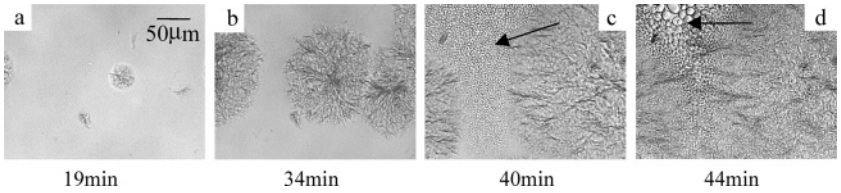

Figure 13. OM pictures of a blend with 15 wt % POM, cured at 145 °C: isothermal crystallization followed by RIPS. The arrow indicates the phase separation in the epoxy-rich phase.

Vv setup, both polarizers are parallel, so both RIPS (i.e., refractive index fluctuation) and crystallization (i.e., orientation correlations due to the presence of crystal aggregates) can lead to an increase of the scattered light intensity. In an Hv setup, where both polarizers are perpendicular, the main contribution to the scattering intensity comes from orientation correlations and hence the crystallization of POM. So we can conclude that the first intensity increase after 30 min of isothermal curing is associated with the RIPS. Fifteen minutes later, the increase of the Hv signal indicates the occurrence of isothermal crystallization in the POM-rich phase. The evolution of the Vv intensity is partially distorted since part of the scattering due to the phase morphology occurs at too small angles behind the beam catcher (in particular when the rapidly coalescing epoxy-rich particles reappear after the apparent phase dissolution) and does not allow for a more detailed discussion. The reported time scales correspond well with the times of RIPS and isothermal crystallization extracted from optical microscopy data (see arrow in Figure 11). The morphology development induced by RIPS is similar to that for the blend of 20 wt % POM cured at 180 °C. However it all happens more slowly because of the slower cure reaction. Table 2 gives an overview of the onset times of RIPS and isothermal crystallization, of the mechanism of demixing, as deduced from SALLS and OM, and finally of the resulting morphology after 4 h of curing at 150 °C. As mentioned, the onset times of RIPS are larger when the cure temperature is lowered to 150 °C, compared to the curing at 180 °C, since the reaction rate is slowed at lower temperatures. Conversion measurements at 150 °C revealed a slightly lower conversion degree at the moment of phase separation (not shown here) for 10 and 20 wt % POM, when compared with the corresponding values of curing at 180 °C, supporting UCST-demixing behavior. The onset of isothermal crystallization has a minimum at 15 wt % POM and increases with increasing amount of POM due to a more pronounced partial miscibility, which can be derived from the occurrence of "apparent phase dissolution". For the same reason, the time difference between RIPS and isothermal crystallization, increases with increasing amount of POM. Blends with 5 and 10 wt % POM did not show isothermal crystallization of POM at 150 °C. Obviously, crystallization in the small droplets needs to be induced homogeneously and this only happens at a large degree of supercooling (at about 80 °C, according to Figure 10).

3.2.2. Curing at 145 °C. Blends cured at 145 °C were prepared in exactly the same way as those cured at 150 °C. Instead of an isothermal curing temperature of 150 °C, 145 °C was taken as T_{cure}. Optical microscopy reveals that in this case isothermal crystallization precedes the liquid−liquid-phase separation. Figure 13 displays the growth of the spherulites in a homogeneous blend of 15 wt % POM. Phase separation occurs in the amorphous zone between the spherulites that started to grow earlier. First a cocontinuous structure is observed (Figure 13c), later this structure breaks up in epoxy droplets (Figure 13d), as indicated with an arrow and is similar to the phase separation in blends with a low POM concentration and discussed for curing and demixing at 180 °C. For every blend composition, the isothermal crystallization precedes the phase separation, which occurs in an epoxy-enriched volume. The sequence of both processes can also be clearly observed with isothermal SALLS measurements. Figure 14 shows the integrated intensity of the scattered light as a function of time for a 15 wt % POM blend. The scattering intensity of the melt was subtracted from both the Vv and Hv signal. After 12 min, an increase in the Hv and Vv signal is observed, indicating the occurrence of isothermal crystallization. The increase in the Vv intensity is larger than that of Hv because the Vv signal contains, besides a signal related to orientation correlations (anistropic scattering), also (isotropic) scattering due to the spherulites being imbedded in a matrix with a different refractive index. This isotropic contribution from refractive index fluctuations should not be confused with scattering that may have been produced by liquid−liquid phase separation. After 36 min of curing, a sharp increase of the Vv signal represents the start of RIPS as at this stage no discontinuity or extra contribution is seen in the Hv intensity. A plot of the azimuthally averaged scattered light intensity (Vv set up) as a function of q can be seen in Figure 15. The scattering maximum associated with spinodal demixing can clearly be identified first at large q and later it increases in intensity and shifts to lower angles (Figure 15a). The intensity increase during the time period (first 40 min) where only isothermal crystallization occurs, is comparatively weak and is magnified in Figure 15b. An overview of the results of the different blend compositions is given in Table 3. A decrease of the onset time of crystallization is observed with

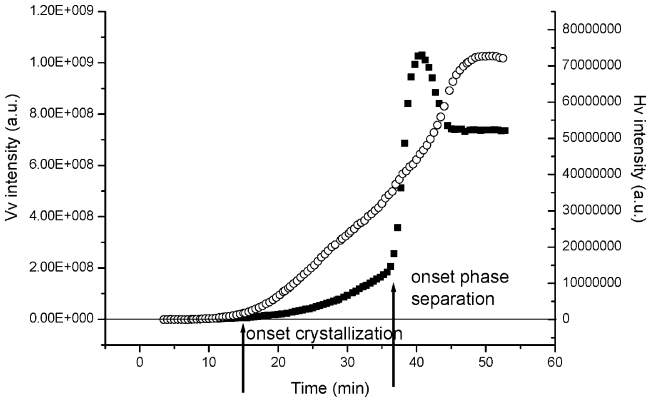

Figure 14. Intensity vs time plot of a blend with 15 wt % POM, cured for 1 h at 145 °C, obtained with SALLS: Vv (closed symbols) and Hv (open symbols) signals. Mind the difference in scale between Vv and Hv signals.

Table 3. Overview of the Onset Times of RIPS and Isothermal Crystallization during Curing at 145 °C

wt % POM	onset time of phase separation (min) (± 0.5 min)	onset time of isothermal crystallization (min) (± 0.5 min)
5	32.6	22.0
10	33.7	17.0
15	36.1	16.0
20	35.9	10.0
30	37.0	9.0

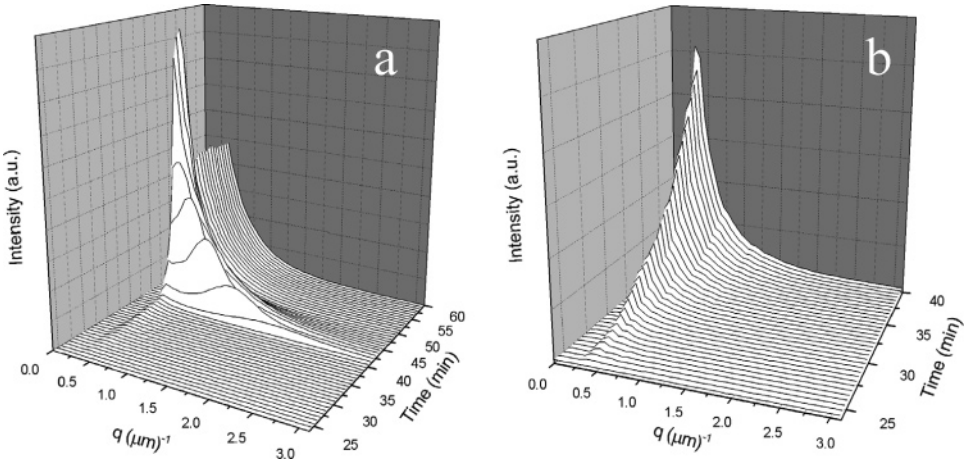

Figure 15. Intensity vs q plot for a blend with 15 wt % POM during curing at 145 °C: (a) from 25 until 60 min of curing, (b) from 25 until 40 min of curing (zoomed in).

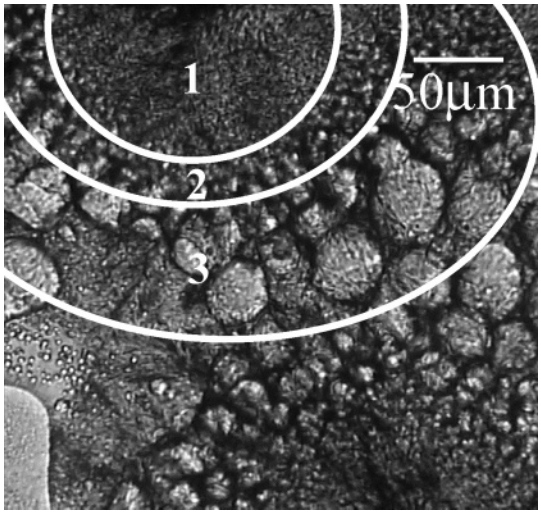

Figure 16. OM picture of growing spherulites in a blend with 15 wt % POM, cured at 145 °C. Different numbers point to different phase-separated structures. A gradient of phase-separated structures is visible.

increasing POM content, as expected from both kinetic and thermodynamic considerations. The lower the dilution of the crystallizable species, the higher the crystallization rate can be because less foreign species need to migrate away from the crystal growth front and the diffusion of the crystallizable species toward the growth front is facilitated. Second, the depression of the equilibrium melting point reduces with an increase of the concentration of the crystallizable polymer. Accordingly, the supercooling increases with increasing POM concentration for crystallization at a given fixed temperature.

An interesting phenomenon is depicted in Figure 16 showing a blend with 15 wt % POM, cured at 145 °C. This picture shows a spherulite that grew during the isothermal curing reaction. The isothermal crystallization extracts POM from the amorphous layer around the growing spherulites. As a consequence, phase separation starts in the volumes distant from the spherulites, since in this zone a relatively large amount of POM is still present. Volumes closer to the crystallization growth front demix later. Accordingly, inspection of the phase-separated structure along the growth path of the spherulites reveals a time gradient of different phase-separated structures with more evolved phase-separated morphologies at larger distances from the spherulites center. Moreover, when the spherulite sweeps through the phase-separated structure the phase morphology development is arrested, since the epoxy droplets are locked in, thus enhancing the gradient of phase-separated structures. To indicate this gradient the spherulite in Figure 16 is divided in three zones. Zone one contains the part of the spherulite that grew in the homogeneous blend. Zone two indicates the part where the phase separation could reach the stage of small droplets after initial spinodal decomposition. The epoxy-rich holes at an even larger distance from the spherulite center represent the volumes that started to phase separate first and of which the phase morphology development was interrupted the latest by crystallization (zone three). Figure 16 hence shows a structure where the droplets become bigger with increasing distance from the spherulites center. This phase morphology gradient has also consequences for the growth rate of the spherulites: an *increase* of the growth rate is observed when volumes are entered that exhibit a more evolved phase separation, obviously because of the POM enrichment in one of the phases. In other words, the crystal growth front selectively follows the pathway set up by the spatial arrangement of the POM enriched phase and increases its progression rate with increasing degree of POM enrichment, i.e., the further away from the spherulite nucleus.

4. Conclusions

The phase-separation behavior of blends consisting of 4,4′-diaminodiphenylsulfone cured diglycidyl ether of bisphenol A with polyoxymethylene cured at 180, 150, or 145 °C was investigated by means of SALLS, optical microscopy, and SEM.

Curing results in reaction-induced phase separation (RIPS), which was studied for blends with different amounts of POM at curing temperatures above (180 °C) and below (150 and 145 °C) the melting temperature of POM (T_m = 168 °C). At 180°C samples demix according to the spinodal decomposition mechanism. Three different final phase morphologies were observed at the end of curing. Blends with 5 and 10 wt % POM display a particle/matrix morphology. The 15 wt % POM blend forms a cocontinuous morphology, where both phases exhibited secondary phase separation. 20 up to 30 wt % POM blends have a phase-inverted structure. Viscoelastic effects clearly interfere when the blends with 15 and 20 wt % POM phase separate. Furthermore, curing leads to changes in the refractive indices of the phases, occasionally resulting in "apparent phase dissolution", which disappears at the onset of secondary phase separation. Secondary phase separation also enhances the interfacial tension between the primary phases, resulting in an inflated phase coarsening process or the appearance of more rounded phase boundaries.

By lowering the curing temperature below the melting point of POM, isothermal crystallization interferes with the RIPS. Curing at 150 °C results in RIPS preceding the isothermal crystallization. In a first step, phase separation occurs in a similar way as for blends cured at 180 °C, but at a certain moment isothermal crystallization of POM starts in the POM-rich phase. When a cure temperature of 145 °C is used, the order of both processes is reversed. POM-spherulites are formed in the miscible blend before phase separation sets in. During spherulite growth, RIPS occurs in the amorphous zone between the spherulites and a gradient in phase-separated structures develops.

Acknowledgment. S.G. thanks the Institute for the Promotion of Innovation through Science and Technology in Flanders (IWT-Vlaanderen) for the Ph.D. grant. B.G. is a postdoctoral fellow of the Fund for Scientific Research Flanders (FWO−Vlaanderen). S.G. thanks G. Vanden Poel for fruitful discussions.

References and Notes

(1) Williams, R. J. J.; Rozenberg, B. A.; Pascault, J. P. *Adv. Polym. Sci.* **1997**, *128*, 95−156.
(2) Ishii, Y.; Ryan, A. J. *Macromolecules* **2000**, *33*, 158−166.
(3) Girard-Reydet, E.; Sautereau, H.; Pascault, J. P.; Keates, P.; Navard, P.; Thollet, G.; Vigier, G. *Polymer* **1998**, *39*, 2269−2279.
(4) Kim, B. S.; Chiba, T.; Inoue, T. *Polymer* **1995**, *36*, 67−71.
(5) Oyanguren, P. A.; Frontini, P. M.; Williams, R. J. J.; Girard-Reydet, E.; Pascault, J. P. *Polymer* **1996**, *37*, 3079−3085.
(6) Oyanguren, P. A.; Frontini, P. M.; Williams, R. J. J.; Vigier, G.; Pascault, J. P. *Polymer* **1996**, *37*, 3087−3092.
(7) Chen, J. L.; Chang, F. C. *Macromolecules* **1999**, *32*, 5348−5356.
(8) Oyanguren, P. A.; Galante, M. J.; Andromaque, K.; Frontini, P. M.; Williams, R. J. J. *Polymer* **1999**, *40*, 5249−5255.
(9) Chen, J. L.; Chang, F. C. *Polymer* **2001**, *42*, 2193-2199.
(10) Yamanaka, K.; Inoue, T. *Polymer* **1989**, *30*, 662−667.
(11) Kim, B. S.; Chiba, T.; Inoue, T. *Polymer* **1995**, *36*, 43−47.
(12) Ishii, Y.; Ryan, A. J.; Clarke, N. *Polymer* **2003**, *44*, 3641−3647.
(13) Elliniadis, S.; Higgins, J. S.; Clarke, N.; McLeish, T. C. B.; Choudhery, R.; Jenkins, S. *Polymer* **1997**, *38*, 4855−4862.
(14) Jiang, X.; Zhang, Y.; Zhang, Y. *J. Polym. Sci., Part B: Polym. Phys.* **2004**, *42*, 1181−1191.
(15) Huang, Y. P.; Woo, E. M. *Polymer* **2001**, *42*, 6493−6502.
(16) Guo, Q.; Thomann, R.; Gronski, W.; Thurn-Albrecht, T. *Macromolecules* **2002**, *35*, 3133−3144.
(17) Guo, Q.; Harrats, C.; Groeninckx, G.; Reynaers, H.; Koch, M. H. J. *Polymer* **2001**, *42*, 6031−6041.
(18) Guo, Q.; Harrats, C.; Groeninckx, G.; Koch, M. H. J. *Polymer*, **2001**, *42*, 4127−4140.
(19) Vanden Poel, G.; Goderis, B.; Groeninckx, G. *Polymer*, to be submitted for publication.
(20) Vanden Poel, G.; Goossens, S.; Goderis, B.; Groeninckx, G. *Polymer* **2005**, *46*, 10758−10771.
(21) Schut, J.; Stamm, M.; Dumon, M.; Galy, J.; Gérard, J. F. *Macromol. Symp.* **2003**, *202*, 25−35.
(22) Zafeiropoulos, N. E.; Schut, J.; Pohlers, A.; Stamm, M.; Gérard, J. F. *Macromol. Symp.* **2003**, *198*, 345−353.
(23) Zhang, J. N.; Zhang, Z. L.; Zhang, H. D.; Yang, Y. L. *Phys. Rev. E.* **2001**; *64*; art. No 051510.
(24) Wang, M.; Yu, Y.; Wu, X.; Li, S. *Polymer* **2004**, *45*, 1253−1259.
(25) Tao, Q.; Gan, W.; Yu, Y.; Wang, M.; Tang, X.; Li, S. *Polymer* **2004**, *45*, 3505−3510.
(26) Yu, Y.; Wang, M.; Gan, W.; Tao, Q.; Li, S. *J. Phys. Chem. B* **2004**, *108*, 6208−6215.
(27) Tanaka, H. *J. Phys. (Paris): Condens. Matter* **2000**, *12*, 207−264.
(28) Tanaka, H.; Koyama, T.; Araki, T. *J. Phys.: Condens. Matter* **2003**, *15*, 387−393.
(29) Faust, R. C. *Proc. Phys. Soc. B* **1955**, *68*, 1081.
(30) Sexto, G.; Hoechst, A. G. In *Polymer Handbook*, 3rd ed.; Brandrup, J., Immergut, E. H., Eds.; John Wiley and Sons: New York, 1989; pp V87−V99.
(31) Clarke, N.; McLeish, T. C. B.; Jenkins, S. D. *Macromolecules* **1995**, *28*, 4650−4659.
(32) Riccardi, C. C.; Borrajo, J.; Williams, R. J. J. *Polymer* **1994**, *35*, 5541−5550.
(33) Remiro, M.; Riccardi, C. C.; Corcuera, M. A.; Mondragon, I. *J. Appl. Polym. Sci.* **1999**, *74*, 772−780.
(34) Kamal, M. R. *Polym. Eng. Sci.* **1974**, *14*, 231−239.
(35) Sourour, S.; Kamal, M. R. *Thermochim. Acta* **1976**, *14*, 41−59.
(36) Bonnet, A.; Pascault, J. P.; Sautereau, H.; Taha, M.; Camberlin, Y. *Macromolecules* **1999**, *32*, 8517−8523.
(37) Vanden Eynde, S.; Mathot, V.; Koch, M. H. J.; Reynaers, H. *Polymer* **2000**, *41*, 3437−3453.
(38) Everaert, V.; Groeninckx, G.; Aerts, L. *Polymer* **2000**, *41*, 1409−1428.

MA052742O